ICAS 2021 SHANG HAI
International Council of the Aeronautical Sciences
32nd Congress of the International Council of the Aeronautical Sciences
September 6-10, 2021
Pudong Shangri-La, Shanghai, China

MECHANISMS OF NATURAL LAMINAR-TURBULENT TRANSITION ON AN UNSWEPT WING IN SUPERSONIC FLIGHT

Chuvakhov P.V. [1,2], Fedorov A.V.[1], & Pogorelov I.O.[1,2]
[1]Moscow Institute of Physics and Technology (MIPT), 9 Institutskiy per., Dolgoprudny, 141701, Russia
[2]Central Aerohydrodynamic Institute (TsAGI), 1 Zhukovskogo Str., Zhukovsky, 140180, Russia

Abstract

Two main sources of disturbances are considered that are capable of triggering transition to turbulence over a thin parabolic-airfoil wing of a supersonic flight vehicle: atmospheric turbulence and acoustic noise radiated by the turbulent boundary layer on a fuselage. Physics-based direct numerical simulation is performed to find which source dominates.

Keywords: laminar-turbulent transition, receptivity, supersonic boundary layer, direct numerical simulation

1. Introduction

Laminar-turbulent transition is one of key problems of fundamental fluid dynamics and applied aerodynamics of flight vehicles of new generation, such as green airplanes with natural and/or artificial laminarization, and supersonic airplanes with low sonic boom level. One of the recent project is the Aerion AS2 business jet [1] having a supersonic unswept laminar wing.

Considering a thin parabolic airfoil, linear stability analysis at the freestream Mach 3 was performed [2]. The e-N computations for a self-similar boundary layer showed that the N-factor envelope of the first mode has maximum in the mid-chord region. The thicker the airfoil, the closer the station of maximum amplification to the leading edge. In accord with the amplitude method [3], this result promises the laminar flow all over the airfoil provided no turbulization occurs upstream of that station. The conclusion of [2] was confirmed by direct numerical simulations of small disturbances on a thin supersonic airfoil [4].

Transition on smooth surfaces starts with the receptivity stage where external disturbances excite normal modes of unstable boundary layers [5]. It remains unclear which disturbance leads to transition in a realistic supersonic flight. Bushnell [6] summarized the possible sources of transition. In a clean atmosphere, the following two main sources should be considered.

The former source is atmospheric turbulence. It was shown [7] that for many practical cases, the instability length-scale lies in the inertial interval or the viscous dissipation interval, where turbulence depends on the two parameters only: kinematic viscosity ν_∞^*, that can be taken from the standard atmosphere, and the dissipation rate ε^*, which was documented for various weather conditions. In a wide range of Mach numbers and flight altitudes, one-order uncertainty in ε^* leads to a marginal error in the predicted transition onset: $|(\Delta x/x)_t| < 17\%$. The velocity perturbations due to atmospheric turbulence are quite small even in the case of storm weather conditions.

The latter source is acoustic noise from the turbulent boundary layer on the fuselage surface. Acoustic waves radiated by the turbulent boundary layer at Mach 2.5 were investigated in [8] using direct numerical simulations. It was found that the acoustic field is dominated by waves having a certain front angle with standard deviation of about 10%. This angle is associated with turbulent sources moving in the boundary layer at supersonic speeds relative to the outer inviscid flow. The rms value of pressure fluctuations is provided to be constant in the far field. Frequency spectra are also available. Therefore, Ref. [8] provides sufficient data to estimate acoustic waves incident onto an unswept wing of a supersonic aircraft similar to Aerion AS2.

In the present paper, we treat the both cases numerically in the framework of Navier–Stokes equations. To be consistent with [4] and save computational resources, we consider a parabolic airfoil of 10% thickness flying at Mach 3 and altitude 20 km. According to the standard atmosphere,

the Reynolds number based on the airfoil chord $L^* = 5m$ is $Re_{\infty.L} = 27.205 \cdot 10^6$ and freestream temperature is $T_\infty^* = 230\ K$. Under these flow conditions, the N-factor envelope of the first mode has maximum at the station $x^*/L^* \approx 0.2$ [4].

2. Problem formulation

2.1 Numerical method

The Navier–Stokes equations are solved using the in-house solver, which implements an implicit finite-volume shock-capturing method with second-order approximation in space and time. A Godunov-type total-variation-diminishing (TVD) scheme with a Roe approximate Riemann solver is used. Reconstruction of the dependent variables at grid cell boundaries is performed using a third-order WENO (weighted essentially non-oscillatory) scheme. Newton and generalized minimal residual methods are used to solve an algebraic system of equations that approximates the partial differential equations. Despite the dissipative nature of the TVD scheme, it is feasible to simulate unstable disturbances in supersonic and hypersonic boundary layers using sufficiently fine computational grids (e.g. [9]). In particular, nonlinear oblique breakdown of a wave train at Mach 3 [10] agrees well with the results of [11], which were obtained using a high-order numerical method.

Present computations were carried out on high-performance multiprocessor computer clusters using a parallel version of HSFlow. The MPI technology and PETSc library of linear algebra routines were employed. Initially structured grids were split up into multiple zones with node-to-node interzone connectivity. More details on the solver can be found in [12].

2.2 Problem specification

Consider a laminar flow past a sharp parabolic airfoil in a supersonic free stream of speed U_∞^*, density ρ_∞^* and temperature T_∞^*. Hereafter asterisks denote dimensional quantities and '∞' marks free-stream quantities. The governing equations are solved in a nondimensional form relative to the corresponding free-stream values, while pressure $p = p^*/(\rho_\infty^* U_\infty^{*2})$. The characteristic length scale is the airfoil chord $L^* = 5\ m$. The nondimensional airfoil shape is $y_w = 2\tau x(x-1)$, where $\tau = 0.1$ is the thickness of the airfoil.

Consider a three-dimensional (3-D) computational domain of Cartesian topology. Its bottom face corresponds to the airfoil upper surface where $(u, v, w) = 0$ and $T_w(x)$ is fixed corresponding to adiabatic wall temperature distribution. The basic flow comes through the left and top faces ('inlet'), and leaves the domain through the right face ('outlet'). The dependent variables are fixed at the inlet and are linearly extrapolated out of the domain at the outlet. The flow is considered as periodic in the spanwise (z) direction.

The free-stream Mach number is 3, the Reynolds number is $Re_{\infty.L} = \rho_\infty^* U_\infty^* L^*/\mu_\infty^* = 27.205 \cdot 10^6$, and freestream temperature is $T_\infty^* = 230\ K$. The viscosity coefficient μ is calculated using Sutherland's formula

$$\mu \equiv \frac{\mu^*}{\mu_\infty^*} = \frac{T_\infty + T_S^*}{T_\infty^* + T^*}\left(\frac{T^*}{T_\infty^*}\right)^{1.5} \equiv \frac{1 + T_S}{1 + T}\,T^{1.5},$$

where $T_S^* = 110.4\ K$. The specific heats ratio and Prandtl number are constants: $\gamma = 1.4, \mathrm{Pr} = 0.72$.

The basic (steady-state laminar) flow past the entire airfoil is computed as a time advancement of unsteady equations to the state when the residual is small, $\sim 10^{-13}$, and the flow field variables change within 10^{-12} over a unit time interval. To reduce computational costs, the disturbance field is simulated in a subdomain $x < 0.42$. The outlet boundary with its buffer region is shifted to the new location $x = 0.42$. This shift does not perturbed the original flow.

The computational grid is clustered toward the leading edge and the wall providing about 125 grid lines across the boundary layer based on criterion $\delta_{0.99}$ for $x > 0.05$. The grid resolves the dominant wavelength in x and z direction with about 40 grid nodes that is sufficient based on our previous experience in direct numerical simulations of boundary-layer disturbances.

Having obtained a 2-D steady state solution, it is extruded in third dimension providing the base field for 3-D computations. Then, the boundary conditions for disturbances are imposed on the left inflow boundary, and the perturbed flow field evolves with about 314 time steps per the period of the dominant wave, $2\pi/\omega_0$. The dimensions of the final 3-D grid are $1451 \times 351 \times 187$.

2.3 Atmospheric turbulence

To simulate atmospheric turbulence, the disturbance vector is imposed on the inlet boundaries as a stochastic signal that consists of plane monochromatic vortical waves with random phase shifts φ_i

$$\vec{V}' \equiv (u', v', w') = \sum_{i=0}^{N} \sqrt{2q_i}\vec{\sigma}_i \sin\left(\vec{k}_i\left(\vec{x} - \vec{U}_\infty t\right) + \varphi_i\right)$$
$$T' = 0, p' = 0$$

Here $\vec{\sigma}_i$ is a unit direction of velocity fluctuation associated with the i-th harmonic, while $\vec{k}_i = k_i\vec{d}_i$ is the wave vector whose unit direction $\vec{d}_i$ is random and uniformly distributed over a sphere of unit radius. The velocity fluctuations are small, and their continuity leads to the orthogonality condition $(\vec{\sigma}_i \cdot \vec{d}_i) = 0$. The wave numbers k_i are evenly spaced over the segment $[k_{min}, k_{max}] = [100, 300]$ at the step Δk: $k_i = k_{min} + i \cdot \Delta k, k_N = k_{max}$. The interval $[k_{min}, k_{max}]$ covers the instability range predicted by the linear stability theory. The central circular frequency of this range is $\omega_0 \approx 197.7$.

This modeling of the vortical disturbance field is similar to that reported in [13], but it accounts for the dispersion relation, $\omega = k_x$, relevant to vortical waves travelling in a uniform flow of $\vec{U}_\infty = (1,0,0)$. Because of spherical distribution of the wave-vector directions $\vec{d}_i$, the frequency interval $\omega_i = k_{i,x} \in [0; 300]$ starts from zero frequency and it is not filled uniformly.

The powers q_i of each harmonic correspond to the discretized von Karman power density spectrum (as suggested in [13]) using the quantitative normalization based on the classical measurements [14] of the inertial interval of turbulence:

$$q_i = E_i \cdot \Delta k,$$
$$E_i = A\frac{(k_i/k_e)^4}{1 + 2.4(k_i/k_e)^{17/6}} \cdot f_\eta(k_i) f_{cut}(k_i),$$
$$A = \alpha \cdot 2.4^{17/6} \cdot \frac{\varepsilon^{2/3}}{k_e^{5/3}},$$
$$f_\eta = \exp\left[-\left(\frac{12k_i}{k_\eta}\right)^2\right],$$
$$f_{cut} = \exp\left[-\left(4\max\left(\frac{k_i}{k_{cut}} - 0.9, 0\right)\right)^3\right],$$

where $k_e = 1$ is the characteristic wave number of large-scale turbulence; $\alpha = 1.7$ [14]; $k_\eta = 2\pi(\nu^3/\varepsilon)^{-0.25}$ is the Kolmogorov's wave number; $k_{cut} = 2\pi/l_{cut}$, $l_{cut} = 2\min(\max(dy, dz, 0.3h_{max}) + 0.1d_w, h_{max})$, d_w is the distance to the wall, $h_{max} = \max(dx, dy, dz)$, dy and dz are local grid steps in the inlet boundary.

Following to [15], the worth the weather conditions, the more powerful the atmospheric turbulence. We consider the case of severe atmospheric turbulence where the factor A is maximal. The worst weather conditions correspond to the value of $\varepsilon^* = 0.06\ m^2/s^3$ [15]. This results in:

$$\alpha\varepsilon^{2/3} = \alpha\left(\varepsilon^* \cdot \left(\frac{{u_\infty^*}^3}{L^*}\right)^{-1}\right)^{2/3} \approx 9.2 \cdot 10^{-7}$$

Running ahead of the results, we intend to show that atmospheric turbulence unlikely leads to transition for the considered problem. Thus, we choose the worst weather case with $\alpha\varepsilon^{2/3} = 10^{-6}$.

Figure 1 illustrates verification of the numerical module providing 3-D disturbance field of atmospheric turbulence in a cube at $t = 0$. To recover spectrum from the constructed disturbance field, its 3-D Fourier transform is performed. The all wave vectors are sorted by their length, and then the power spectral density is restored by averaging the harmonics power over the wave number segments of different length Δk_i (fig. 1b).

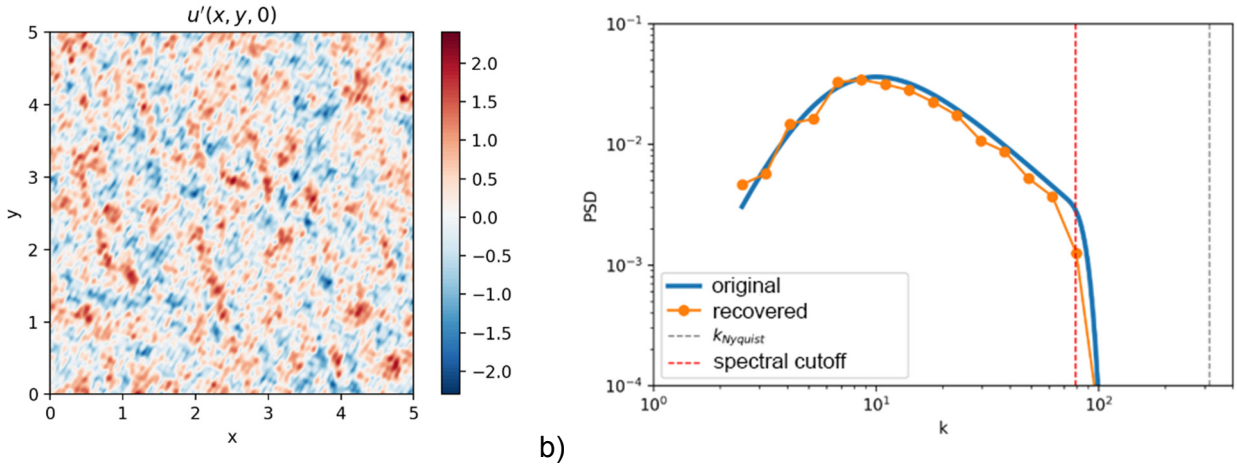

a) b)

Figure 1 – The generated disturbance field $u'(x,y,z)$ of atmospheric turbulence at $z=0$ (a) and comparison of the original and recovered power spectral densities (b)

2.4 Acoustic noise

Statistical properties of acoustic waves radiated by turbulent boundary layer were estimated in [16]. The direct numerical simulation [8] confirmed the dominance of acoustic waves in the disturbance field induced by the turbulent boundary layer at the freestream Mach number 2.5. The radiated waves were associated with sources, which moved in a turbulent boundary layer supersonically relative to the outer flow at speed $U_b \approx 0.4U_e$. The dominant-wave vector was oriented at an angle ψ to the wall, which was expressed in terms of U_b as

$$\cos\psi = \frac{1}{M_e(U_b-1)}.$$

Deviation ΔU_b from U_b is estimated using the correlation coefficient for pressure fluctuations reported in [8]. This coefficient is approximated by Gaussian function at $\Delta t_0 = 2\pi/\omega_0$:

$$C_{pp} = C_{pp,0} + B\cdot\exp\left(-\frac{1}{2\sigma^2}(\Delta x-\Delta x_0)^2\right).$$

The rms deviation is $\sigma = 0.044$ in the vicinity of ω_0 where the far-field disturbances spectrum attains maximum. Using this data the uncertainty in U_b is estimated as 10%. Assuming that U_b is approximately the same at close Mach numbers M_e, the dominant wave angle is evaluated as

$$\cos\psi \approx \frac{1}{M_e(U_b\pm\sigma-1)} \approx \frac{1}{M_e(U_b-1)}\left(1\mp\frac{\sigma}{U_b-1}\right) = \cos\psi_b \mp \Delta(\cos\psi_b)$$

In the considered herein case of $M_e = 3$, its value is $\psi_b = 123.75° \pm 2.78°$. Therefore, it can be assumed that acoustic waves have a fixed angle ψ in a broad frequency band.

Considering slow and fast acoustic wave separately, the turbulent boundary layer radiates slow waves of the angle $\psi_b - \pi = -56.25°$ with respect to x-axis, with the 'attack' angle $\theta > 0$ counterclockwisely. Dealing with 3-D acoustic waves that are generated on the fuselage surface and fall onto the wing, the geometrical interpretation of the acoustic field relative to the fuselage axis results in the 'sweep' angle $\tilde{\beta} = \psi_b - \pi = -56.25°$, while the 'attack' angle is $\theta = 0°$. An elementary monochromatic wave having the pressure amplitude ϵ is expressed as

$$(u',v',w',p',T') = \left(\hat{u},\hat{v},\hat{w},\hat{p},\hat{T}\right)\cdot\sin\left(\vec{k}\cdot\vec{x}-\omega t+\varphi\right).$$

$$\hat{p} = \epsilon,\ \hat{T} = (\gamma-1)M_\infty^2\epsilon,$$
$$\hat{u} = -\epsilon\, M_\infty\cdot\cos\theta\cos\tilde{\beta} = -\epsilon M_\infty\cdot\cos\tilde{\beta},$$
$$\hat{v} = +\epsilon\, M_\infty\cdot\sin\theta = 0,$$
$$\hat{w} = -\epsilon\, M_\infty\cdot\cos\theta\sin\tilde{\beta} = -\epsilon M_\infty\cdot\sin\tilde{\beta},$$

Here $\vec{k} = k_\infty\left(\cos\tilde{\beta},0,\sin\tilde{\beta}\right)$, $k_\infty = \omega/(\cos\tilde{\beta}-1/M_\infty)$ and φ is a phase shift.

Similarly to the case of atmospheric turbulence, a stochastic signal in a frequency band $\omega\in[100,300]$ is constructed as a sum of elementary harmonics spaced evenly with the step $\Delta\omega$

$$p' = \sum_i \sqrt{2\Phi(\omega_i)\Delta\omega}\,\sin\left(\vec{k}_i\vec{r} - \omega_i t + \varphi_i\right).$$

Phase shifts φ_i are randomly and uniformly distributed over $[0,2\pi]$. The pressure disturbance amplitude $\epsilon = \sqrt{2\Phi(\omega_i)\Delta\omega}$ is calculated using the power spectral density reported in [8] (see fig. 2a) accompanied by root-mean-square value ${p'_{rms}}^*/\tau_w^* \approx 0.4$ ($p'_{rms}/c_f \approx 0.2$ in dimensionless form). The friction coefficient c_f can be estimated using the turbulent boundary layer parameters on the fuselage surface from where the acoustic waves comes onto the wing mid span. Using the geometry of Aerion AS2 vehicle [1] and determining the direction of acoustic energy propagation (about $\phi \approx 13.2°$, see fig. 3), acoustic waves are radiated from the station $x_0^* \approx 9.57\ m$ measured from the fuselage nose tip. Using the theoretical solution [17] for the boundary layer past a cone, we estimate the value of c_f over a flat plate at x_0^* to be $1.136 \cdot 10^{-3}$ (less than the cone's value by the factor of $\sqrt{3}$), which leads to $p'_{rms} \approx 2.272 \cdot 10^{-4} \approx 2.86 \cdot 10^{-3}\ p_\infty$. Applying this value to the frequency spectrum [8], we close the formulation for the acoustic field imposed on the inflow boundary.

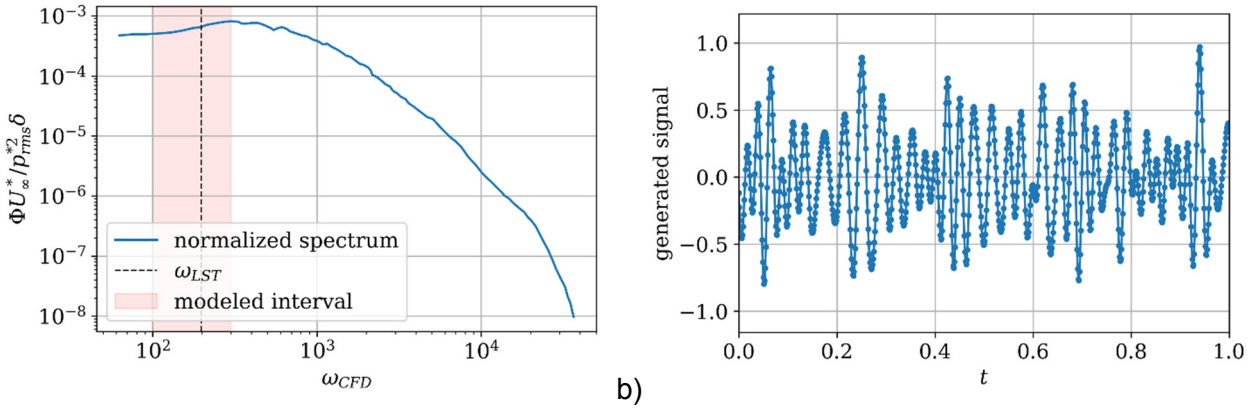

a) b)

Figure 2 – Power spectrum from [8] (a) and a segment of generated random signal for the modeled spectrum interval (b, rms amplitude is approx. 0.366).

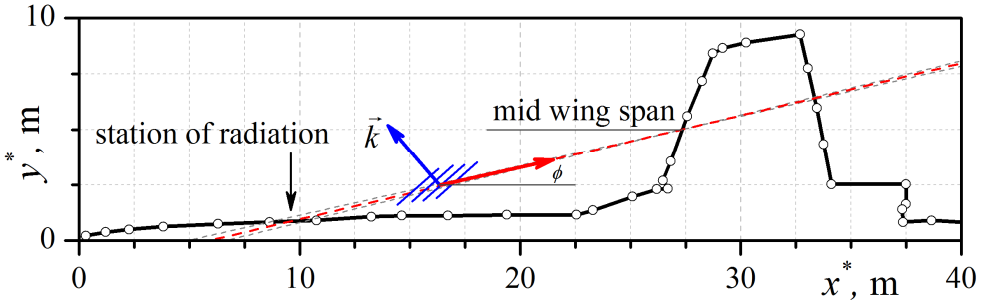

Figure 3 – Schematic of plane acoustic waves radiated from the fuselage to propagate to the mid span of the wing (sample vehicle geometry is based on Aerion AS2 design [1]).

It is important to emphasize that the fuselage should be treated as a cylindrical source of disturbances rather than a flat one. If this is the case, the amplitude of the radiated acoustic waves attenuate as a square root of the radial distance from the fuselage axis. Thus, the value of p'_{rms} near the wing leading edge is lower by $\sqrt{y_2^*/y_1^*}$ than that for the flat source. Considering the geometry in fig. 3, the acoustic amplitude should be reduced by $\sqrt{5.8}$ to give $p'_{rms} \approx 9.434 \cdot 10^{-5} \approx 1.19 \cdot 10^{-3} p_\infty$. We will proceed with the case of flat source where the acoustic noise is most powerful.

2.5 Post processing of numerical solutions

Having been imposed at the left inflow boundary, disturbances evolve downstream. Upon time interval $\Delta t \approx 0.6$, transient effects associated with the disturbance switching on becomes negligible and statistics of the disturbed flow is considered as stationary over the wing airfoil. Starting from $t = 0.6$, the wall pressure disturbances $p'_w(t,x,z)$ are stored up to the time instant $t = 1.85$. Then the data are analyzed using 2-D Fourier transform in time t and spanwise coordinate z at several x-stations normalized by the total number of sample points used, $N_t \cdot N_z$: $\Im p'_w(\omega,x,\beta)$.

3. Results

3.1 Disturbance fields

In the case of acoustic forcing, external perturbations penetrate into the boundary layer and grow downstream. They reach nearly maximum amplitude by the station $x \approx 0.2$ where they stop growing and start either attenuate or break to turbulent spots. The latter arise from local bumps of random forcing which excite more powerful patches of the boundary layer disturbances. For the past of a characteristic flow time $\Delta t = 1$ from forcing start, a quasi-stationary regime sets in. This means that turbulent spots appear from time to time at $x > 0.25$ at random z-stations. This process does not stop. The spots become larger as they propagate downstream. The wall pressure disturbance field due to acoustic forcing is illustrated in fig. 4.

Figure 5 shows the distribution of average friction coefficient over the airfoil surface. The disturbed distribution first deflects from the non-disturbed at $x \approx 0.1$, though next downstream the deviation between those two changes marginally. Eventually, the disturbed distribution goes away at $x \approx 0.27$, which points to the transition onset. In accord with the intermittency model (see e.g. [Narasimha]) transition begins with excitation of isolated turbulent spots which grow in size propagating downstream. Ultimately, the spots merge with each other resulting in a well-developed turbulent boundary layer.

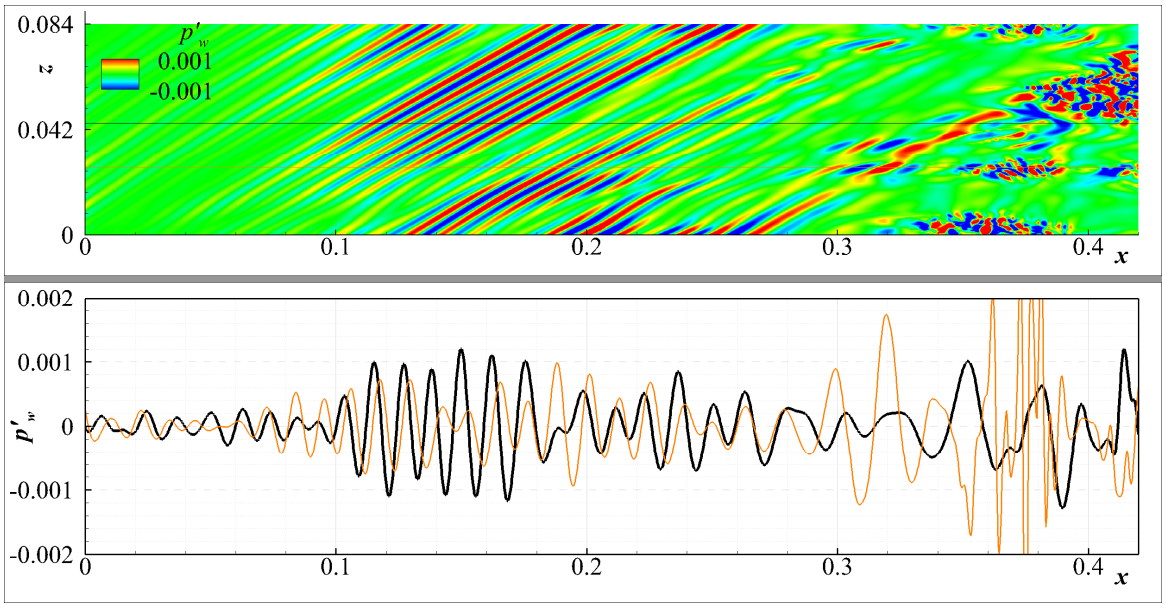

Figure 4 – Wall pressure disturbance field, $p'_w(x, z)$ and its distributions along two lines $z = const$. Acoustic disturbances.

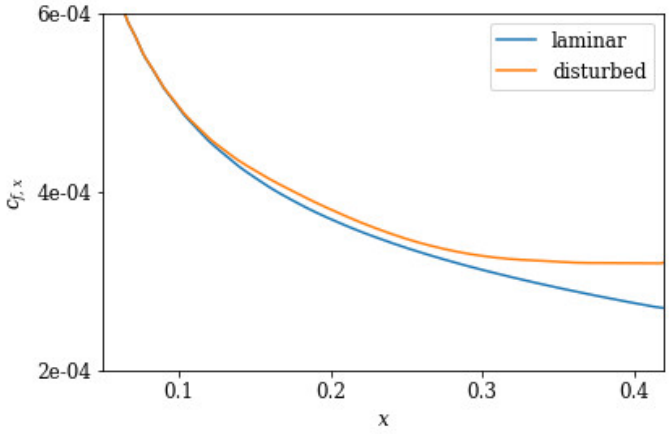

Figure 5 – Distribution of time-zpanwise-averaged friction coefficient along the wall

In contrast to the case of acoustic forcing, the atmospheric turbulence excites the boundary-layer disturbances of much smaller amplitudes (compare data in figs. 4 and 6). In the leading-edge region, the disturbance field is dominated by waves of relatively large length. Their amplitude decrease

slightly as they move downstream. Meanwhile, shorter waves with oblique fronts become visible past the station $x \approx 0.1$. They resemble those dominating in the case of acoustic forcing. Their downstream amplification allows us to assume that these waves may be relevant to the first mode. Downstream from the station $x \approx 0.22$ the short waves attenuate while the long waves take over again. In general, the disturbance intensity remains low throughout the airfoil and turbulent spots are not observed.

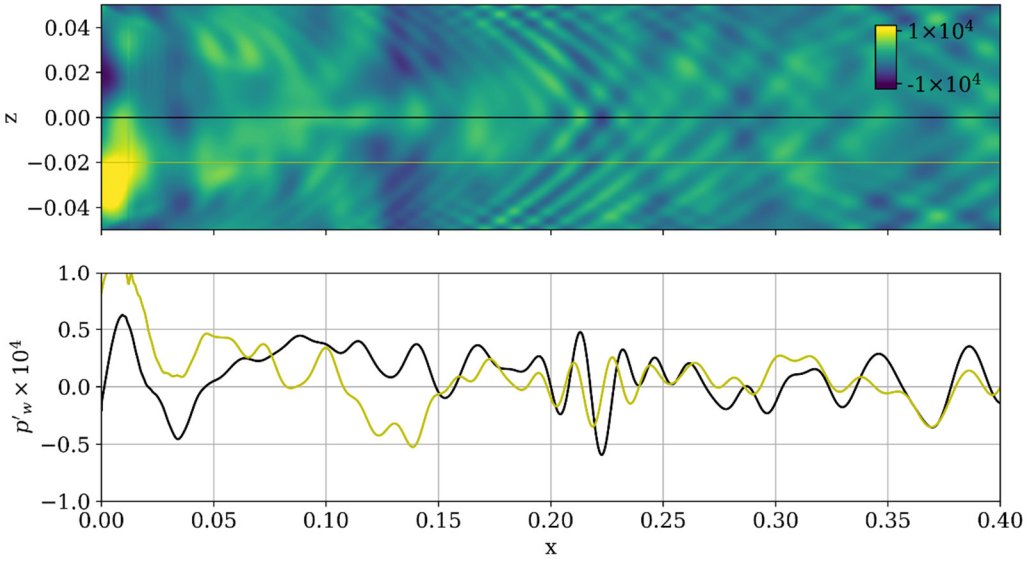

Figure 6 – Wall pressure disturbance field, $p'_w(x,z)$ and its distributions along two lines $z = const$. Atmospheric turbulence.

3.2 Disturbance spectra

As expected, spectral contents of the boundary-layer disturbances are quite different (see fig. 7). In the case of acoustic forcing, the initial spectrum consists of elementary oblique of a fixed front angle. Therefore, it is localized near an inclined line in the $\omega - \beta$ plane. This spectral shape holds up to the station $x = 0.2$ indicating that the boundary-layer disturbance evolves in accord with the linear theory. Note that the spectrum maximum moves to lower frequencies and reaches the value $\omega \approx 200$ at $x = 0.2$, which agrees with prediction of the linear stability theory for the first-mode instability [4]. Nonlinear features are visible at $x > 0.2$. The spectrum line becomes wider ($x = 0.3$) and ultimately breaks into a broadband spectrum at $x = 0.4$, with zero-frequency component being well distinguished. This station corresponds to the formation of turbulent spots. In accord with the data shown in fig. 4, the spectra clearly indicate that the transition onset is located at $x \approx 0.25$.

In the case of atmospheric turbulence forcing, the initial spectrum is quite different because of random direction of the wave vector. It is broad in β and occupies a long wave region including $\beta = 0$ (fig. 7, left, $x = 0.1$). The waves cover the frequency band from 0 to 300, thereby containing frequencies relevant to the case of acoustic forcing. No oblique waves of $|\beta| \approx 500$ are visible at $x = 0.1$. Further downstream though they appear at $x = 0.2$, slightly amplifies to $x = 0.3$ and then attenuates to $x = 0.4$. These harmonics do not dominate the disturbance flow, they are too weak to trigger turbulent spots. Therefore, the spectra do not broaden and attenuate nearly monotonically. Note that the spectra resemble V-shape in the stations $x = 0.2, 0.3, 0.4$), indicating the presence of oblique waves observed in fig. 6. The wave-front angles can be estimated by the inclination of spectral V-legs as

$$\arctan\left(\frac{\beta}{\omega}\right) = \arctan\left(\frac{d\beta}{d\omega}\right) \approx \arctan\left(\frac{1000}{350}\right) \approx 71°.$$

This value agrees well with the wave-front angles of the dominant first mode wave predicted by the linear stability theory [2,4]: from $69°$ to $70°$.

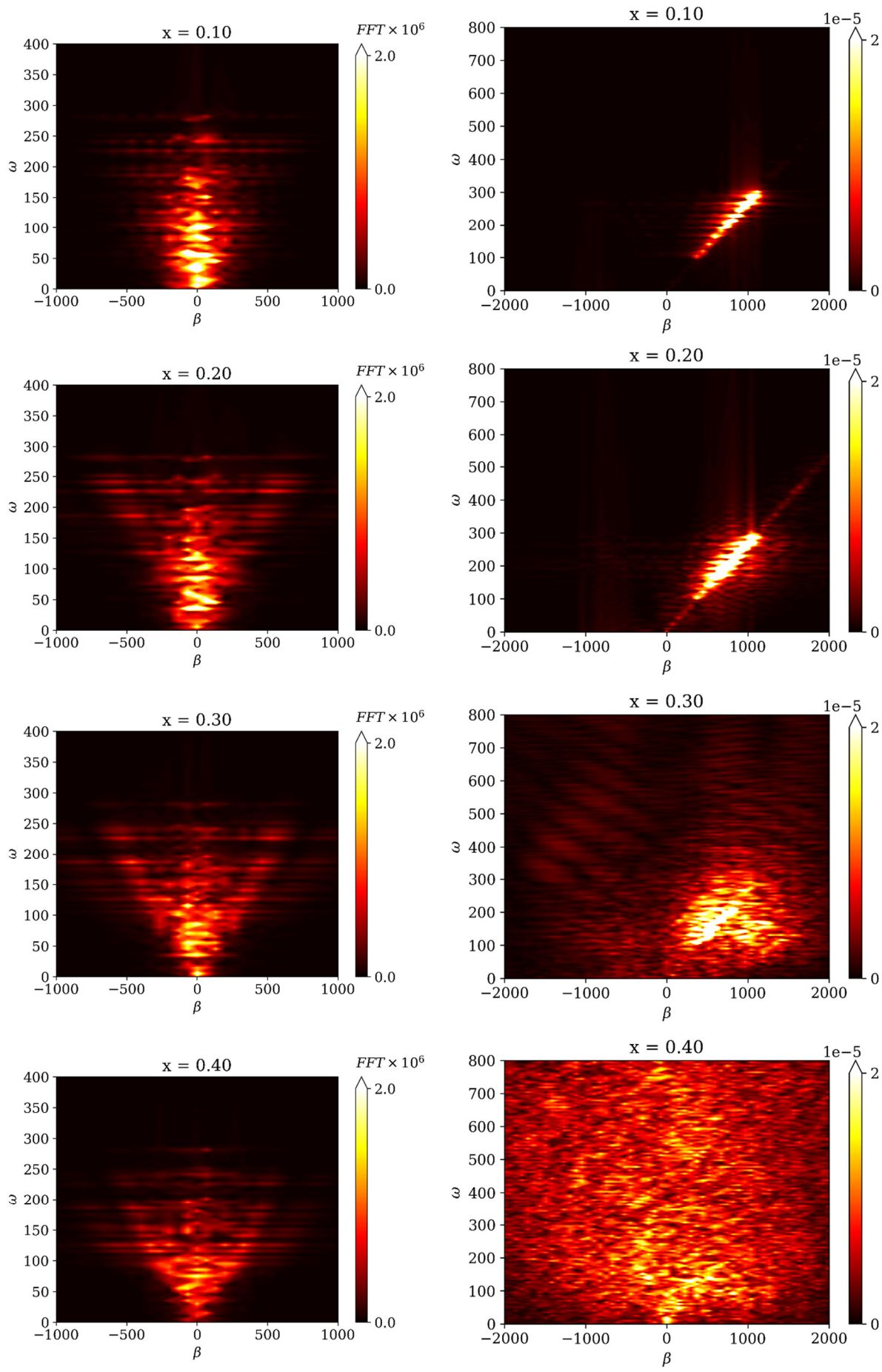

Figure 7 – Two-dimensional spectra of wall pressure disturbances $p'_w(t,z)$ at four streamwise stations. Left column – atmospheric turbulence, right column – acoustic disturbances.

4. Conclusion

Numerical simulation of realistic environmental disturbances penetrating into a supersonic boundary layer on an unswept wing with thin parabolic airfoil at the free-stream Mach number 3 shows that boundary layer transition to turbulence is most likely to occur because of acoustic noise radiated by the turbulent boundary layer on the fuselage surface. Even under the storm weather conditions, the atmospheric turbulence at 20 km altitude weakly affects the boundary layer and does not cause the nonlinear breakdown.

An obvious way to laminarize such a wing is to reduce the acoustic field generated by the turbulent boundary layer on the fuselage surface. This could be shaping and smoothing of the surface, suction the boundary layer or devices breaking coherent turbulent structures.

Future work is to support the above conclusion by more accurate simulations of the fuselage-induced acoustic field. It is natural to consider cylindrical waves which amplitude is inversely proportional to the square root of the radial distance from the fuselage symmetry axis. Preliminary estimations show that such acoustic noise should be weaken by $\sqrt{5.8}$ in amplitude for the configuration considered herein.

5. Acknowledgements

The work has been carried out in Moscow institute of physics and technology under the support of Russian Science Foundation (Project no. 19-79-10132) using computing resources of the federal collective usage center Complex for Simulation and Data Processing for Mega-science Facilities at NRC “Kurchatov Institute”, http://ckp.nrcki.ru/.

6. Contact Author Email Address

mailto: pavel_chuvahov@mail.ru

7. Copyright Statement

8. References

[1] Liebhardta B, Lütjensb K, Tracyc RR, et al. Exploring the prospect of small supersonic airliners – a business case study based on the Aerion AS2 jet. *17th AIAA aviation technology, integration, and operations conference*, USA, Denver, Colorado, AIAA paper 2017-3588, 5–9 June 2017.

[2] Fedorov A and Obraz A. The stability analysis of the flow over thin parabolic profile at Mach 3. *Problems of mechanics: theory, experiment and new technologies: abstracts of the XIV all-Russian school-conference of young scientists*, Russia, Novosibirsk – Sheregesh, pp. 143-144, 2020.

[3] Mack LM. *Transition and laminar instability.* NASA-CP-153203, 1977.

[4] Chuvakhov PV, Fedorov AV, Obraz AO and Ilyukhin IM. Disturbance evolution over an upswept wingin a Mach 3 flow. *AIP Conference Proceedings*, Vol. 2351, Paper number 030026, 2021.

[5] Morkovin MV, Reshotko E. and Herbert TH. Transition in open flow systems: a reassessment. *Bull. Am. Phys. Soc.*, Vol. 39 (9), pp. 1–31, 1994.

[6] Bushnell D. Notes on initial disturbance fields for the transition problem. *In: Instability and Transition (ed. M. Y. Hussaini & R. G. Voigt),* pp. 217–232. Springer, 1990

[7] Egorov IV, Fedorov AV, Novikov AV and Chuvakhov PV. The Role of Receptivity in Prediction of High-Speed Laminar-Turbulent Transition. *In Proc.: IUTAM Symposium on Laminar-Turbulent Transition,* London, UK, 2-6th September, pp. 1–11, 2019. To be published in the Springer IUTAM Bookseries.

[8] Duan L, Choudhari MM and Wu M. Numerical study of acoustic radiation due to a supersonic turbulent boundary layer. *J. Fluid Mech.* Vol. 746, pp. 165–192, 2014.

[9] Chuvakhov PV, Fedorov AV and Obraz AO. Numerical simulation of turbulent spots generated by unstable wave packets in a hypersonic boundary layer. *Computers & Fluids*, Vol. 162, pp. 26–38, 2018.

[10]Egorov I, Nguyen N, Nguyen T, Chuvakhov P. Simulation of laminar-turbulent transition using dissipative numerical schemes. *Computational Mathematics and Mathematical Physics*, Vol. 61, pp.254-266, 2021.

[11]Christian SJ. von Terzi MDA and Fasel HF. DNS of Complete Transition to Turbulence via Oblique Breakdown at Mach 3. *AIAA paper* 2008-4398, 2008.

[12]Egorov IV and Novikov AV. Direct numerical simulation of boundary layer flow over a flat plate at hypersonic flow speeds. *Comput. Math. Math. Phys.*, Vol. 56 (6), pp. 1048–1064, 2016.

[13]Adamian DY, Strelets MKh, Travin AK. An efficient method of synthetic turbulence generation at les inflow in zonal rans-les approaches to computation of turbulent flows. *Mathematical models and computer simulations*, Vol. 23 (7), pp. 3–19, 2011.

[14]Pao Y-H. Structure of Turbulent Velocity and Scalar Fields at Large Wavenumbers. *The Physics of Fluids*, Vol. 8 (6), pp. 1063–1075, 1965.

[15]McMinn JD. Extension of a Kolmogorov atmospheric turbulence model for time-based simulation implementation. *AIAA Guidance, Navigation, and Control Conference*, New Orleans, LA, USA, AIAA paper 97-3532, 11–13 August 1997

[16]Laufer J. Some statistical properties of the pressure field radiated by a turbulent boundary layer. *The Physics of Fluids*, Vol. 7 (8), pp. 1191–1197, 1964

[17]Hrubecky HF. An approximate analysis for the turbulent boundary layer thickness on a cone in supersonic flow. *Appl. sci. Res., Section A*, Vol. 11, pp. 441–450, 1963